




Cite this: *RSC Adv.*, 2021, 11, 8134

# Photoluminescent sea urchin-shaped carbon-nanobranched polymers as nanoprobe for the selective and sensitive assay of hypochlorite†

Xin Zhang,<sup>ab</sup> Jian Qu <sup>\*a</sup> and Shou-Nian Ding <sup>\*b</sup>

This work reports donor–acceptor type sea urchin-like carbon nanobranched polymers (SUCNPs). As a novel carbon-based nanomaterial, SUCNPs were effectively synthesized for the first time through a facile and economical solvothermal approach employing uric acid and L-cysteine as nitrogen/sulfur sources. The nitrogen-rich structure of the heterocyclic aromatic polymer led to a blue fluorescence at the excitation/emission maxima of 350/436 nm with robust photostability. SUCNPs showed highly selective ability towards hypochlorite ( $\text{ClO}^-$ ) against other relevant interfering substances. Upon exposure to a growing concentration of  $\text{ClO}^-$ , SUCNPs fluorescence presented a gradual rise with a remarkable blue shift by virtue of the inhibition of photoinduced charge transfer (PCT) process. A linear relationship was established between the fluorescence intensity ratio ( $I_{401\text{ nm}}/I_{436\text{ nm}}$ ) and the  $\text{ClO}^-$  concentration in the range of 0.1–200  $\mu\text{M}$ . The detection limit was as low as 30 nM ( $3\sigma/k$ ). The “turn-on” type nanoprobe was further used in real samples and paper-based analytical chips efficiently, implying its application in a sophisticated and convenient platform.

Received 7th September 2020

Accepted 3rd February 2021

DOI: 10.1039/d0ra07608b

rsc.li/rsc-advances

## 1. Introduction

As a representative reactive oxygen species (ROS), hypochlorite ( $\text{ClO}^-$ ) is capable of reacting with some proteins, DNA, RNA and other biological molecules, which are associated with many irreversible diseases.<sup>1–3</sup> In addition to its physiological function,  $\text{ClO}^-$  is employed as a disinfectant in the pretreatment of drinking water owing to its anti-infection ability.<sup>4</sup> Hence, it is imperative to explore sensitive probes for the assay of  $\text{ClO}^-$  in biological and environmental systems.

To date, diverse analytical approaches have been utilized for the assay of  $\text{ClO}^-$  anions, such as capillary electrophoresis,<sup>5</sup> electrochemiluminescence,<sup>6</sup> electrochemistry,<sup>7</sup> chromatography,<sup>8</sup> and fluorescence.<sup>9</sup> Among these, the fluorescent sensor exhibits superiority in sensitivity and stability, and is regarded as a robust tool. Lately, Wei *et al.* synthesized carbon dots (CDs) from 2,5-diaminobenzenesulfonic acid to detect  $\text{ClO}^-$  and ascorbic acid in living cells and body fluid.<sup>10</sup> Wang *et al.* synthesized B,N-co-doped CDs from adenine and 3-amino-benzene to recognize  $\text{ClO}^-$  in fluorometric and colorimetric manners.<sup>11</sup> Meanwhile, it is meaningful to design “turn-on” mode or colour-tunable fluorescent probes which can respond

to the target with increased signal or in the form of blue/red-shifts. In the field of organic fluorescent probes, D– $\pi$ –A structured molecules are frequently designed to accomplish target-induced emission colour changes through linking electron-rich and electron-poor groups to  $\pi$ -conjugated spacers.<sup>12,13</sup> Inspired by this strategy, we decided to synthesize photoluminescent nanomaterials with similar structures *via* a facile approach for obtaining a high-contrast chromism.

Photoluminescent carbon-based nanomaterials (PCNs) are widely applied in fluorescent sensors owing to their assorted inherent merits, such as remarkable photostability, ultralow cytotoxicity, green synthetic methods, *etc.*<sup>14–16</sup> As large-sized carbon-based nanomaterials, carbon-nanobranched materials have gained tremendous attention recently. For example, Wang *et al.* synthesized coral-like carbon-branched polymers using uric acid and phosphoric acid as precursors by a hydrothermal method for captopril detection.<sup>15</sup> Gao *et al.* synthesized nickel-doped carbon-branched nanomaterials for quercetin detection using nickel(II) acetylacetonate as a metal–carbon source *via* a hydrothermal method.<sup>17</sup> Ola *et al.* synthesized dendritic tin-based carbon nanodendrites by a two-step carbonization and chemical vapor deposition method using tin chloride and acetone as precursors.<sup>18</sup> This progress encouraged us to synthesize such nanostructures and further explore their optical performance. It is well-known that changing the N-doping and S-doping can effectively tune the optical characteristics of carbon nanodots (CDs). Intuitively, doping carbon-nanobranched materials with these elements may also alter their electronic characteristics and surface functional groups

<sup>a</sup>School of Materials Science and Engineering, Yancheng Institute of Technology, Yancheng 224051, China

<sup>b</sup>School of Chemistry and Chemical Engineering, Southeast University, Nanjing 211189, China

† Electronic supplementary information (ESI) available. See DOI: 10.1039/d0ra07608b



and thereby bring about a new phenomenon. Considering this, we decided to make attempts to synthesize N,S-doped carbon-nanobranched materials.

Taking the abovementioned factors into account, we disclose a facile and resource-saving method to synthesize novel N,S-co-doped carbon nano-branched polymers with a sea urchin shape (SUCNPs). The chemical composition, surface valence state and optical properties of this carbon-based nanomaterial were investigated in detail. Interestingly, the SUCNPs exhibited remarkable  $\text{ClO}^-$  targeting ability, with a fluorescent blue-shift and turn-on behaviours. The recognition mechanism related to the photoinduced charge transfer (PCT) process was further validated. Under the optimal conditions, the sensitive nanoprobe was successfully applied in real sample analysis and analytical paper chips.

## 2. Materials and methods

### 2.1 Chemicals and apparatus

The chemicals and apparatus are introduced in the ESI.†

### 2.2 Synthesis of fluorescent SUCNPs

Fluorescent SUCNPs were synthesized *via* a traditional solvothermal approach with uric acid as the nitrogen donor and L-cysteine as the sulfur donor. In brief, uric acid (0.15 g) and L-cysteine (0.15 g) were placed in a mixed solution of water and ethanol with a total volume of 14 mL (1 : 1). The suspension was further ultrasonicated for 15 min to acquire a well-distributed solution. Then, the resulting solution was moved into a poly(tetrafluoroethylene)-lined stainless steel autoclave. After being heated at 185 °C for 4.5 h in an oven, the autoclave was chilled and the inner solution was centrifuged at 8000 rpm for 10 min to remove impurities. The supernatant was kept still in a refrigerator for 3 days to eliminate large fragments. Then, dialysis (1000 Da MWCO) was carried out against deionized water overnight for purification. Eventually, the purified SUCNPs were dried under reduced pressure at 50 °C for one day and dissolved in water again to serve as a stock solution ( $1.4 \text{ mg mL}^{-1}$ ).

### 2.3 Optimizing the experimental conditions

To obtain better analysis performance, the pH value of the testing solution was optimized before the assay. The working solutions of  $\text{ClO}^-$  were freshly prepared by diluting commercially available NaClO with double distilled water to the desired concentrations. In a routine process, 20  $\mu\text{L}$  of SUCNPs ( $1.4 \text{ mg mL}^{-1}$ ), 50  $\mu\text{L}$  of  $\text{ClO}^-$  anion (5.0 mM) and 50  $\mu\text{L}$  of phosphate buffer (50 mM) with different pH values were mixed firstly; then, an appropriate amount of double distilled water was supplemented to achieve a total volume of 500  $\mu\text{L}$ , and the resulting solution was vortexed gently for 2 min. Finally, the obtained testing solutions with various pH values were transferred into a microscale quartz cell and measured by FL spectroscopy.

### 2.4 Fluorescence detection of $\text{ClO}^-$ by SUCNPs

In a normal assay, 20  $\mu\text{L}$  of SUCNPs dispersion ( $1.4 \text{ mg mL}^{-1}$ ) was pipetted into 50  $\mu\text{L}$  phosphate buffer (50 mmol  $\text{L}^{-1}$ ). After

that, as-prepared  $\text{ClO}^-$  solutions with different concentrations were added, and an appropriate amount of double distilled water was supplemented to adjust the sample volume to 500  $\mu\text{L}$ . Subsequently, the sample was vortex-mixed for 2 min and incubated for 5 min to guarantee the reproducibility. FL emission spectra were then collected at the excitation of 350 nm.

The selectivity of SUCNPs was assessed by comparing with some competitive anions, metal ions and other oxidative species, including  $\text{Cu}^{2+}$ ,  $\text{Zn}^{2+}$ ,  $\text{Ni}^{2+}$ ,  $\text{Co}^{2+}$ ,  $\text{Hg}^{2+}$ ,  $\text{F}^-$ ,  $\text{Cl}^-$ ,  $\text{Br}^-$ ,  $\text{I}^-$ ,  $\text{NO}_3^-$ ,  $\text{NO}_2^-$ ,  $\text{SO}_4^{2-}$ ,  $\text{PO}_4^{3-}$ ,  $\text{HPO}_4^{2-}$ ,  $\text{CO}_3^{2-}$ ,  $\text{ClO}_2^-$ ,  $\text{ClO}_4^-$ ,  $\text{H}_2\text{O}_2$ ,  $\cdot\text{OH}$  and  $\text{NO}$ . The concentration of these species was 1 mM, and the corresponding test conditions were similar to the above descriptions.

### 2.5 Analysis of real samples

The nanoprobe was utilized to analyze  $\text{ClO}^-$  concentrations of tap water, wastewater and human serum for the evaluation of its potential applications. The tap water sample was directly obtained from our laboratory and tested without any pretreatment. The wastewater sample was obtained from Lin Tai Paper Mill (Yancheng, China). For the wastewater sample, centrifugation and filtration through a water-phase microporous filter membrane (0.45  $\mu\text{m}$ ) were executed. Ten-fold dilution with phosphate buffer was then performed. EDTA (1 mM) was added to the diluted wastewater as a chelator to capture the interfering ions. The human serum sample was supplied by Southeast University Affiliated Zhongda Hospital (Nanjing, China) and was subjected to 100-fold dilution before testing. The recovery test was performed based on the standard addition method. In brief,  $\text{ClO}^-$  standard working solutions with known concentrations were added to the above real samples, respectively. The fluorescence spectra were measured at the excitation of 350 nm. The recovery was calculated according to eqn (1):

$$\text{Recovery (\%)} = C_{\text{measured}} / (C_{\text{added}} + C_0) \times 100\% \quad (1)$$

where  $C_{\text{measured}}$  is the concentration after addition calculated according to the linear equation,  $C_0$  is the initial concentration in the sample, and  $C_{\text{added}}$  represents the spiked concentration.

### 2.6 Visual detection of $\text{ClO}^-$ on the $\mu\text{PAD}$

The designed pattern was printed on a sheet of chromatography paper using a wax printer. Then, the wax-printed paper was baked in an oven at 150 °C for 1 min to melt the wax so that it could penetrate into the paper and define the hydrophobic barriers. One sheet of the chromatography paper can produce 12  $\mu\text{PADs}$  at a cost of \$0.06 each. Subsequently, an appropriate volume of SUCNPs dispersion was added to the hydrophilic reservoir to evenly adsorb the probes onto the porous fiber. After drying in an oven, the  $\mu\text{PAD}$  was used to detect  $\text{ClO}^-$  (100  $\mu\text{M}$ ) with a UV light.

## 3. Results and discussion

### 3.1 Design and synthesis of SUCNPs

For our SUCNPs, uric acid and L-cysteine served as the carbon-nitrogen and nitrogen-sulfur sources, respectively, and ethanol



was utilized as a stabilizer without any toxic additives during the whole course, enabling environmentally friendly synthesis. In the solvothermal process, the abundant carbonyl, amino, carboxyl and thiol groups on the precursor surfaces underwent condensation, carbonization and polymerization to afford SUCNPs. The ratio of carbon precursors and the reaction time were optimized to achieve a maximum effect at first. As illustrated in Fig. 1A and B, the mass ratio of uric acid and L-cysteine exerted great influence on the FL intensity of the SUCNPs. The FL signal of the SUCNPs increased with increasing mass ratio from 1 : 0 to 1 : 1 (uric acid : L-cysteine, wt%) and then declined when the value exceeded 1 : 1, indicating that the density of the surface state may be lessened with a too high or too low mass ratio. Additionally, compared to the carbon nanostructures with only L-cysteine or uric acid, SUCNPs showed a distinct structural difference (Fig. S1† and 2A), implying that the following photophysical changes may originate from the structural differences. As reported, unusual morphologies could be attained by optimal conditions in which the doping heteroatoms fit the size and active site requirements, which are capable of modulating their photoluminescent properties, involving electronic configuration and passivation groups.<sup>19</sup> It is worth emphasizing here that the reaction time is another critical factor affecting the FL signals. As depicted in Fig. 1C, the FL intensity reached the maximum at the reaction time of 4.5 h and declined in the range of 4.5–6 h. DLS was carried out to explore the growth process of SUCNPs in depth (Fig. 1D–F). The time-dependent hydrodynamic diameters and FL performance imply that

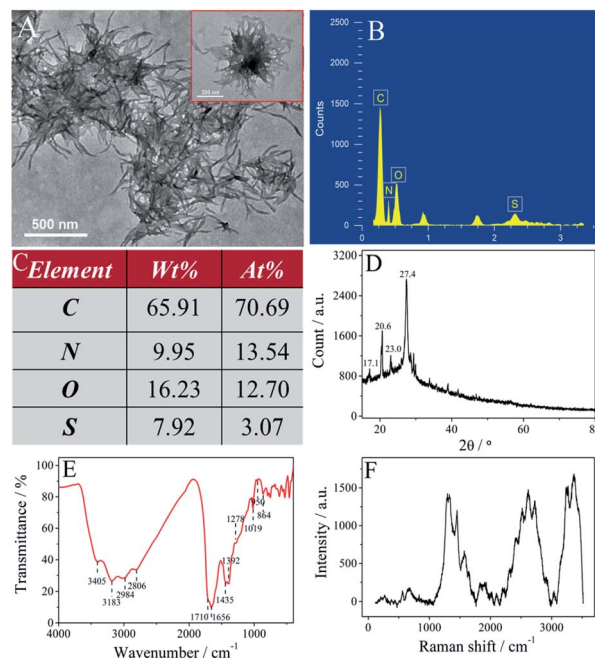


Fig. 2 Characterization of the SUCNPs. (A) TEM, (B) EDS, (C) element contents of C, N, O, S, (D) XRD, (E) FTIR and (F) Raman spectra.

a short reaction time may lead to a low reaction efficiency and insufficient carbonization; in contrast, a longer time may reduce the surface functional groups and the emissive sites, and both conditions would cause a loss of FL intensity. The residue thioether bonds in the as-prepared SUCNPs were expected to react quickly towards  $\text{ClO}^-$ , resulting in FL response through altering the PCT process, originally from the electron-rich groups (such as thioether/amino groups) to the electron-withdrawing groups of SUCNPs (such as carbonyl/carboxyl groups) (Scheme 1).

### 3.2 Characterization of SUCNPs

As shown in Fig. 2A, the SUCNPs have a nano-branched structure and are nearly sea urchin-shaped. The high-magnification TEM image exhibits that the branches are loosely scattered

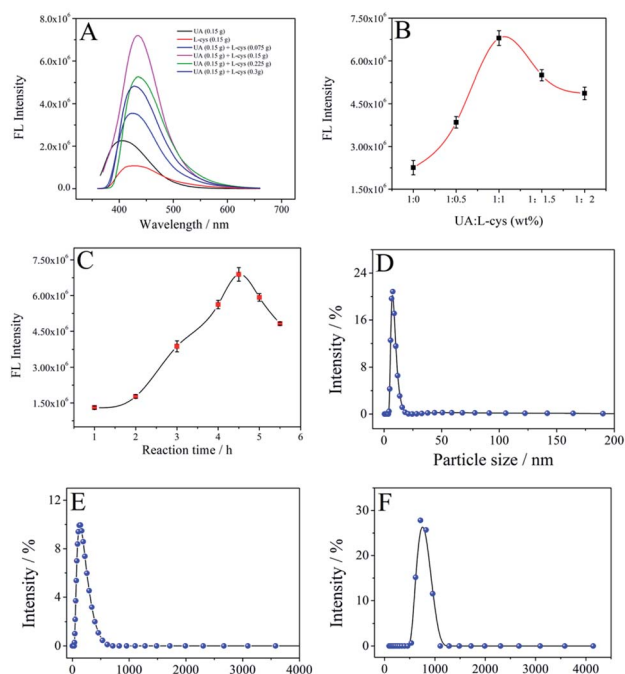
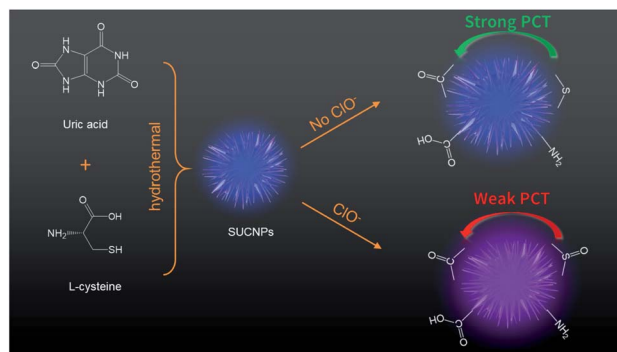


Fig. 1 Effects of the mass ratio of the precursors (A and B) and reaction time (C) on the FL emission intensity of the SUCNPs ( $\lambda_{\text{exc}} = 350$  nm, slit width = 2 nm). The measurements were conducted in triplicate, and each RSD was lower than 5.81%. DLS curves of the SUCNPs at different reaction stages: 1 h (D), 3 h (E) and 4.5 h (F).



Scheme 1 Schematic of the synthesis process of the SUCNPs and the mechanism of fluorescent detection of  $\text{ClO}^-$  by the SUCNPs.



around the core. The average length of these branches is around 226 nm and the mean radius is 9 nm (inset in Fig. 2A). The diameter of a whole SUCNP particle is around 585 nm, slightly smaller than the DLS result (Fig. 1F). This difference originates from the feature in which DLS tests the hydrodynamic diameter with the unconfined structure, different from the dry samples on the carbon support membrane during TEM characterization.<sup>20</sup> The EDS spectrum displays four peaks at 0.27, 0.40, 0.53 and 2.31 keV, consistent with C (70.69 at%), N (13.54 at%), O (12.70 at%) and S (3.07 at%), respectively (Fig. 2B and C). The N/S atomic ratio in the as-prepared SUCNPs is about 4 : 1, which is lower than that in the precursors (5 : 1); this implies that a small portion of N atoms were lost in the synthesis process. The alteration of the N/S atomic ratio may play a vital role in the structural and photophysical transformation. The typical XRD pattern of SUCNPs shows four characteristic diffraction peaks centered at about 17.1°, 20.6°, 23.0° and 27.4°, ascribed to the (220), (311), (102) and (331) planes of buckminsterfullerene (JCPDS no. 44-0558 and 49-1718) and implying the turbostratic structure of the SUCNPs (Fig. 2D).<sup>21</sup>

The bonding mode and organofunctional groups of the SUCNPs were characterized by FTIR spectroscopy. Fig. 2E illustrates two broad bands at 3405 and 3183 cm<sup>-1</sup>, which correspond to the O–H and N–H stretching vibrations. The absorption bands at 2984 and 2806 cm<sup>-1</sup> can be assigned to the C–H stretching vibration mode. The characteristic band at 1710 cm<sup>-1</sup> is attributed to C=O stretching vibration, indicating the presence of carboxylic groups and –CONH– groups. The spectrum also presents the typical bands of aromatic C=N bonds at 1656 cm<sup>-1</sup> and C–N stretching vibrations at 1392–1435 cm<sup>-1</sup>, suggesting that numerous aromatic CN units exist in the SUCNPs. Additionally, the bands in the range of 1019–1278 cm<sup>-1</sup> are assigned to the C–O and C–S stretching vibrations of ether/thioether groups. Thus, it is believed that the surface of the SUCNPs is full of diverse hydroxyl groups, amino groups, amide groups, carboxylic groups and thioether groups, whose skeletons are mainly composed of polycyclic aromatic and heterocyclic rings. Raman spectroscopy is a professional tool to identify the skeleton arrangements of carbon-based materials; particularly, the symmetric vibrations of conjugated C=C/C=N–C bonds in the cyclic skeleton induce intense signals. Three prominent peaks and two weak peaks appeared in the region of 250–3500 cm<sup>-1</sup> of the Raman spectrum (Fig. 2F), related to the heterocyclic aromatic polymer, which is consistent with previous reports.<sup>22,23</sup> The peaks at around 500–1100 cm<sup>-1</sup> and 1100–2200 cm<sup>-1</sup> are attributed to the  $\nu_2$  and  $\nu_1$  vibrations of C=C non-polar bonds and C=N/C=O polar bonds, significantly different from the characteristic D band and G band of the alveolate 2D graphene quantum dots in this range, implying that the SUCNPs are more inclined to be polymer-like structures.<sup>24</sup> The relatively strong peaks at 2200–2900 cm<sup>-1</sup> and 3100–3500 cm<sup>-1</sup> may be due to C–H and N–H/O–H stretching vibrations.<sup>25</sup> All the above results indicate that the SUCNPs are composed of aromatic heterocycles (incorporating C=N moieties) with amino, amide, carboxylic, hydroxyl, thiol, and thioether groups on the surface.

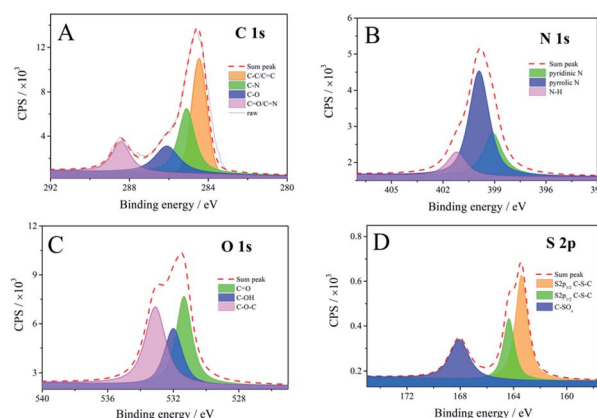


Fig. 3 XPS C 1s (A), N 1s (B), O 1s (C) and S 2p (D) spectra of the SUCNPs.

The XPS survey spectrum (Fig. S2†) shows five prominent peaks at 164, 228, 285, 400 and 532 eV, respectively, which are indexed to the S 2p, S 2s, C 1s, N 1s and O 1s peaks. Semi-quantitative analysis shows that the SUCNPs are composed of C (66.34 at%), N (15.81 at%), O (14.95 at%) and S (2.90 at%), demonstrating that N and S have been richly doped into the carbon skeleton. The C 1s spectrum of SUCNPs can be fitted into four peaks at 284.5, 285.1, 286.1 and 288.4 eV, corresponding to the four components of carbon element, namely C–C/C=C, C–N, C–O and C=O/C=N, manifesting the heterocyclic structure (Fig. 3A).<sup>26</sup> As shown in the N 1s spectrum (Fig. 3B), two distinct peaks at 399.1 and 399.9 eV are ascribed to pyridinic N and pyrrolic N, confirming the sp<sup>2</sup> C=N/sp<sup>3</sup> C–N structure in the polycyclic skeleton.<sup>27</sup> The peak at 401.2 eV is attributed to N–H groups, verifying the presence of amino groups on the surface of the obtained SUCNPs. The O 1s spectrum can be deconvoluted into three peaks at 531.3, 531.9 and 533.1 eV, which are attributed to C=O, C–OH and C–O–C, respectively (Fig. 3C).<sup>28</sup> Additionally, the S 2p spectrum in Fig. 3D displays three peaks at 163.4, 164.3 and 168.1 eV. The first two are indexed to 2p<sub>3/2</sub> and 2p<sub>1/2</sub> C–S–C covalent bonds of thiophene-S in virtue of the spin–orbit couplings, and the last one corresponds to –C–SO<sub>x</sub>– species (x = 1, 2, 3, 4) as sulfonate or sulfate groups.<sup>29</sup> On the basis of these surface state explorations, it can be deduced that the S atoms are inserted into the

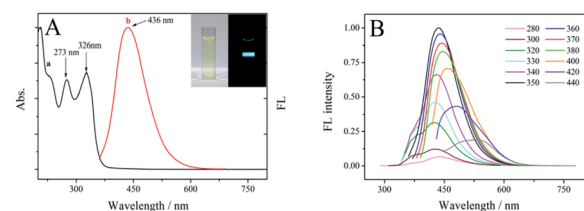


Fig. 4 (A) The normalized UV-vis absorption (a) and FL emission spectra (b) ( $\lambda_{\text{ex}} = 350$  nm) of the SUCNPs. Inset: photographs under daylight and 350 nm UV light. (B) FL emission spectra of aqueous solutions of SUCNPs with various excitation wavelengths. The slit widths were 2 nm.



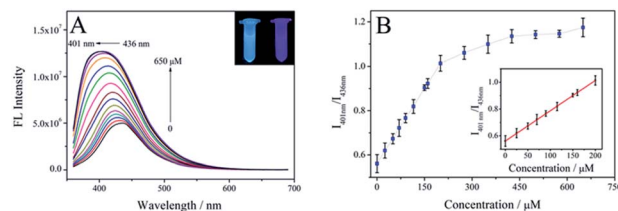


Fig. 5 (A) FL emission spectra of SUCNPs with increasing concentrations of  $\text{ClO}^-$  anions,  $\lambda_{\text{ex}} = 350$  nm, slit width = 2 nm. Inset: photographs of SUCNPs solution and SUCNP solution with the addition of  $\text{ClO}^-$  under UV light (365 nm). (B) Plots of  $I_{401 \text{ nm}}/I_{436 \text{ nm}}$  versus  $\text{ClO}^-$  concentration. Inset: the linear relationship. Error bars are shown for the standard derivation of three tests, and each RSD is lower than 5.13%.

networks mainly in these two forms, and the SUCNPs are highly S-doped, N-enriched heterocyclic nanopolymers.

### 3.3 Optical properties of SUCNPs

The optical properties of the SUCNPs were checked *via* UV-vis absorption and FL emission spectra. Fig. 4A reveals that the SUCNPs possess two evident UV-vis peaks at  $\sim 273$  nm and  $\sim 326$  nm, respectively (curve a). The former peak mainly originates from the  $\pi$ - $\pi^*$  transition of double bonds, such as C=C and C=N, implying a rich electronic conjugate arrangement and verifying the heterocyclic skeleton.<sup>30</sup> The latter peak is mainly derived from the  $n$ - $\pi^*$  transitions of C=O and S=O bonds on the SUCNP surfaces.<sup>31</sup> From the macroscopic view, the light yellow aqueous solution of SUCNPs emitted intense blue luminescence under UV excitation (350 nm, inset of Fig. 4A), and the corresponding FL emission is centered at 436 nm with a Stokes shift of 86 nm (curve b, Fig. 4A).

The photoluminescence behaviours were further studied by altering the excitation wavelength. As illustrated in Fig. 4B, the FL intensity increased gradually as the excitation wavelength shifted from 280 nm to 340 nm, but the peak positions remained almost unchanged. It is deduced that relatively uniform surface states resulting from the N-enriched and S-doped polymers dominate the FL behaviour, with a relatively

high-energy excitation. Self-passivated activated groups wrapped on the surfaces cause surface-activated sites to form between the  $\pi^*$  and  $\pi$  energy levels.<sup>32</sup> When the excitation was over 350 nm, the emission wavelength moved from 436 nm to 530 nm, presenting “excitation-dependent” behaviour. Meanwhile, the intensity also declined gradually. This phenomenon indicates that the nonuniformity of the particle sizes and unique morphology tune the optical behaviour at this range, similar to most previously reported carbon dots.<sup>33,34</sup> As a whole, the stage-variation characteristic of the FL spectra should be the synergistic effect of the surface electron energy traps and the carbogenic core. According to these results, the excitation wavelength of 350 nm was chosen as the optimum wavelength. Moreover, the absolute quantum yield of the SUCNPs was 10.79% under this excitation.

Fig. S3† depicts the influences of pH and ionic strength on the FL intensity of the SUCNPs. The FL emission was stable in a wide range (pH 5–10). The intensity decreased gradually under extremely acidic and alkaline conditions (Fig. S3A†) because an overly acidic or alkaline environment would alter the surface states by the protonation–deprotonation process of the carboxyl and amino moieties. The FL of SUCNPs with varied concentrations of NaCl was studied to evaluate the influence of the ionic strength. FL signals were stable even when the concentration of NaCl was up to 200  $\mu\text{M}$ , demonstrating that the SUCNPs possess good salt-tolerance (Fig. S3B†).

### 3.4 Optimization of method

The pH value is a determining factor for the recognition process between the SUCNPs and  $\text{ClO}^-$ . Fig. S4† illustrates the FL responses of the SUCNPs towards 500  $\mu\text{M}$   $\text{ClO}^-$  at different pH values (5–10); the optimal pH value is 7.0, so it was chosen for the following analysis.

### 3.5 $\text{ClO}^-$ anion detection using SUCNPs as fluorescence probes

The feasibility of utilizing the SUCNPs as a photoluminescent nanoprobe was explored *via* FL measurements. In a preliminary

Table 1 Comparison of various fluorescent probes for  $\text{ClO}^-$  detection

Type of probe	Synthesis precursors	Linear range ( $\mu\text{M}$ )	LOD (nM)	Ref.
CDs	Catechol	0.1–10	30	35
CDs	Hongcaitai	0.05–15	15	36
GSH-CDs	Prickly pear cactus juice	10–90	16	37
P, N-CDs	Adenosine-5'-triphosphate	5–200	280	38
CDs	Citric acid	2.5–100	1500	39
	Urea			
CDs	2,5-Diaminobenzenesulfonic acid	0.1–100	83	10
CDs	Sweet pepper	0.1–10	50	40
		10–300		
B, N-CDs	3-Aminobenzene boronic acid monohydrate	0.1–1000	$45.57 \pm 0.75$	11
	Adenine			
Eu complex loaded carbon nanotube	Carbon nanotube	0.1–0.8	90	41
SUCNPs	Uric acid	0.1–200	30	This work
	L-Cysteine			



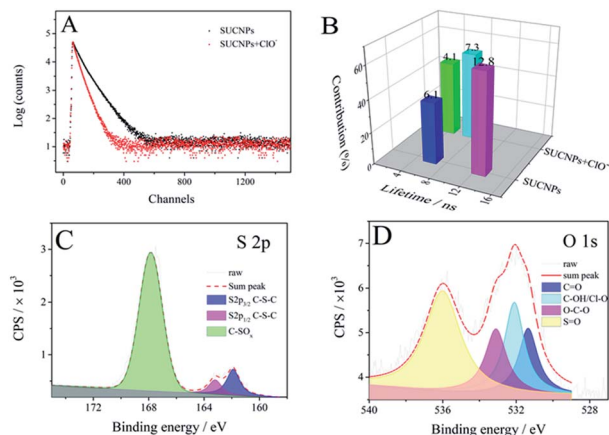


Fig. 6 (A) FL decay and (B) FL lifetimes of the SUCNPs with or without ClO<sup>−</sup> (650 μM). (C) S 2p and (D) O 1s XPS spectra of SUCNPs–ClO<sup>−</sup>.

study, ClO<sup>−</sup> exerted a significant blue-shift effect on the SUCNPs. As shown in the inset of Fig. 5A, the FL of the SUCNPs solution turned violet from its intrinsic blue after adding 650 μM ClO<sup>−</sup> anions. Thus, the quantitative analysis of ClO<sup>−</sup> was further investigated using SUCNPs as a photoluminescent probe. Fig. 5A displays the FL changes of SUCNPs solution with various concentrations of ClO<sup>−</sup> anions. With the increment of the target, the FL intensity enhanced gradually and reached a saturation at about 425 μM. Meanwhile, the maximum emission peak moved from 436 nm to 401 nm. It worth noting that 2.5-fold enhancement of FL intensity was achieved in this course. The FL ratio values ( $I_{401\text{ nm}}/I_{436\text{ nm}}$ ) exhibited a linear relationship with the ClO<sup>−</sup> concentration (0.1–200 μM,  $R^2 = 0.998$ , Fig. 5B). The detection limit was calculated based on  $3\sigma/k$  according to previous literature reports.<sup>3</sup> FL measurements for blank samples were carried out with five parallel tests to estimate the standard deviation ( $\sigma$ ).  $k$  represents the slope of the linear regression equation. The detection limit was calculated to be 30 nM. The detailed calculation process is shown in the ESI.† Moreover, a comparison with the assay performance of other known ClO<sup>−</sup> probes was carried out (Table 1). The results indicate that the SUCNPs possess a wider detection range and lower detection limit, verifying that the SUCNPs are robust FL nanoprobes for ClO<sup>−</sup> with high sensitivity.

### 3.6 Mechanism of ClO<sup>−</sup> anion detection by the FL SUCNPs

To gain insight into the blue-shift phenomenon in FL sensing, the FL decays of the SUCNPs in the presence and absence of

ClO<sup>−</sup> were examined (Fig. 6A). The fraction contributions of two related time-resolved decay lifetimes,  $\tau_1$  and  $\tau_2$ , were summed up in Fig. 6B. The average lifetime of the SUCNPs was 9.08 ns according to calculations, and that after ClO<sup>−</sup> addition was 5.34 ns. This change confirms the increase of the radiative decay rate, indicating that the surface defects were influenced through the combination with ClO<sup>−</sup>. Further investigation was carried out to reveal the interaction between the probe and target. As depicted in Fig. 6C and Table 2, the –SO<sub>x</sub> content was enhanced outstandingly after reaction with ClO<sup>−</sup>, indicating that the divalent sulfur at the surface edge may be oxidized into sulfoxide. Compared with pure SUCNPs, the area percentage of S=O in the O 1s spectrum also increased (Fig. 6D), which further verifies the increase of the oxidized sulfoxide groups in the presence of ClO<sup>−</sup>. Based on the above characterization, the SUCNPs can be regarded as a  $\pi$ -conjugated heterocyclic skeleton with electron-donating groups (amino groups, hydroxyl groups and thioether) and electron-withdrawing groups (carboxyl, carbonyl groups) at the surfaces. Upon excitation, a strong PCT process proceeded *via* the push–pull effect from the electron-donating groups to the electron-withdrawing groups. After treatment with ClO<sup>−</sup>, the electron-donating thioether moiety was converted to an electron-deficient sulfoxide moiety by oxidation.<sup>42</sup> Thereby, the PCT process was dramatically inhibited, leading to a high-contrast FL blue shift. As shown in Fig. S5,† after the addition of 200 μM ClO<sup>−</sup>, the main absorption of the SUCNPs at 326 nm blue shifted to 319 nm, consistent with the absorption results of previous reports regarding PCT-based CD chemosensors.<sup>43</sup> The blue shift phenomena of absorption and emission are in good agreement with the suppression of the PCT process.<sup>44</sup>

To study the autooxidation possibility of SUCNPs, the SUCNPs solution was exposed to air for 21 days in the dark. As shown in Fig. S6A and B,† the FL performance remained stable during air exposure; the RSD of the FL intensity at maximum emission peak was 1.45%, verifying that the SUCNPs solution was difficult to oxidize by oxygen in air. Further, the SUCNPs solution after 21 days of air exposure exhibited similar sensing ability towards ClO<sup>−</sup> compared with the fresh SUCNPs, confirming that the thiol groups had not yet been auto-oxidized by oxygen during air exposure (Fig. S6C†). Meanwhile, the SUCNPs solution was purged with O<sub>2</sub> for 30 min to further evaluate the influence of oxygen on the SUCNPs. As depicted in Fig. S6D,† no discernible difference was found between the FL spectra of the normal SUCNPs solution and O<sub>2</sub>-purged SUCNPs solution. For the O<sub>2</sub>-purged SUCNPs sample, the sensing ability towards ClO<sup>−</sup>

Table 2 Chemical compositions, percentages of peak areas, and binding energies of S element in the S 2p XPS spectrum

Sample	% Area (BE of S 2p in eV)		S 2p	Mass content (%) S total
	S 2p <sub>3/2</sub>	S 2p <sub>1/2</sub>		
SUCNPs	46.9 (163.4)	24.9 (164.4)	28.2 (168.1)	2.90
SUCNPs + ClO <sup>−</sup>	11.9 (162.1)	6.3 (163.2)	81.8 (167.9)	2.71

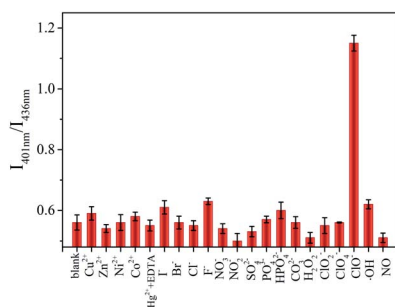


Fig. 7 Selectivity of the SUCNPs for  $\text{ClO}^-$  over other species. The measurements were conducted in triplicate, and each RSD was lower than 4.8%.

was similar to that of the pure sample. These results demonstrate that autooxidation did not occur when the SUCNPs were exposed to air.

In addition, only a slight FL decrease (2.84%) was found after 2 months of storage under daylight (Fig. S6D†), and no floating or precipitates were observed during this storage; this indicates that the obtained SUCNPs solution was not sensitive to daylight, and it possesses good stability in ambient conditions.

### 3.7 Selectivity of SUCNPs

The selectivity of the SUCNPs for the  $\text{ClO}^-$  assay was estimated by studying the FL responses towards representative metal ions, anions and other oxidative species ( $\text{Cu}^{2+}$ ,  $\text{Zn}^{2+}$ ,  $\text{Ni}^{2+}$ ,  $\text{Co}^{2+}$ ,  $\text{Hg}^{2+}$ ,  $\text{I}^-$ ,  $\text{Br}^-$ ,  $\text{Cl}^-$ ,  $\text{F}^-$ ,  $\text{NO}_3^-$ ,  $\text{NO}_2^-$ ,  $\text{SO}_4^{2-}$ ,  $\text{PO}_4^{3-}$ ,  $\text{HPO}_4^{2-}$ ,  $\text{CO}_3^{2-}$ ,  $\text{ClO}_2^-$ ,  $\text{ClO}_4^-$ ,  $\text{H}_2\text{O}_2$ ,  $\text{OH}^-$  and  $\text{NO}$ ). As illustrated in Fig. 7, a significant response was obtained only by the addition of  $\text{ClO}^-$ , and the other interfering species induced neglectable changes. As shown in Fig. S7,† different from  $\text{ClO}^-$ , the addition of  $\text{ClO}_2^-$  and  $\text{ClO}_4^-$  did not bring about any change to the FL of the SUCNPs. The reason may be that  $\text{ClO}^-$  ions possess stronger oxidizability than  $\text{ClO}_2^-$  and  $\text{ClO}_4^-$ , which can be inferred from their standard electrode potentials ( $E^\theta$ ). Meanwhile, it is also worth noting that  $\text{OH}^-$  and  $\text{H}_2\text{O}_2$  quenched the FL intensity markedly. However, the ratio value of  $I_{401 \text{ nm}}/I_{436 \text{ nm}}$  was not affected in this situation. More importantly, considering the fact that  $\text{H}_2\text{O}_2$  cannot coexist with  $\text{NaClO}$  in a genuine sample

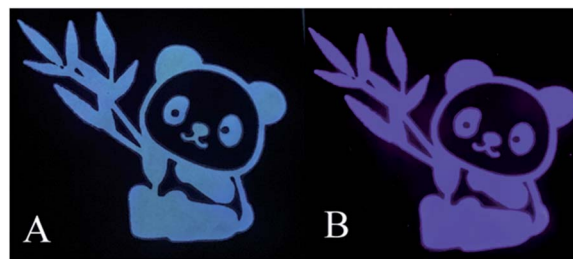


Fig. 8 Photographs of the SUCNPs test paper before (A) and after (B) exposure to the  $\text{ClO}^-$  anions (100  $\mu\text{M}$ ) under UV light excitation ( $\lambda_{\text{ex}} = 365 \text{ nm}$ ).

because an oxidation–reduction reaction would occur when they met, the interference from  $\text{H}_2\text{O}_2$  could be neglected. These results validate that the probe meets the selectivity requirement for  $\text{ClO}^-$  assays in practical application.

### 3.8 Real samples

Recovery tests were carried out with tap water, wastewater and human serum samples using the standard addition method. The added concentrations of  $\text{ClO}^-$  in the samples were calculated based on the above linear equation, and the measured data are summarized in Table 3. The recovery was within the range of 93.7–107.3%, and the RSD values were less than 3.39%, implying that potential interferences in the matrix would not affect the assay performance. The corresponding data are shown in Fig. S8.† These results confirm that the SUCNPs probe is practical for  $\text{ClO}^-$  assays in real samples.

### 3.9 Visual detection of $\text{ClO}^-$ on the $\mu\text{PAD}$

To achieve fast and portable detection of  $\text{ClO}^-$ , chromatography paper was chosen to prepare SUCNPs test papers by a soaking and drying process. As shown in Fig. 8A, the pattern appeared bright blue under a 365 nm UV lamp. After exposure to  $\text{ClO}^-$  (100  $\mu\text{M}$ ), the fluorescent color changed to violet (Fig. 8B), consistent with the phenomenon in solution (inset of Fig. 5A). This finding indicates that the dried SUCNPs still possessed sensing ability for  $\text{ClO}^-$ ; thus, this test paper can work in flexible ways to be implemented in different analytical tasks.

## 4. Conclusions

In summary, a sea urchin-like carbon nanobranched polymer was synthesized with various electron donor–acceptor groups on its surface. Rich nitrogen contents (13.54%) and appropriate sulfur doping flexibly tuned the electronic distribution and surface chemical reactivity. In virtue of the oxidative transformation of thioether into sulfoxide groups, triggered by  $\text{ClO}^-$ , the SUCNPs displayed a “light-up” fluorescence enhancement towards  $\text{ClO}^-$ , accompanied by an evident visible color change. The related recognition mechanism was characterized carefully and indicated a weakened process of intramolecular charge transfer. The limit of detection was 30 nM, which is superior to those of most current methods for  $\text{ClO}^-$  analysis. Additionally,

Table 3 Determination of  $\text{ClO}^-$  anions in tap water, wastewater and human serum samples

Sample	Added (nM)	Measured (nM)	Average (nM)	Recovery (%)	RSD ( $n = 3$ )
Tap water	30.0	30.9 30.6 30.1	30.5	101.7	1.32
Waste water	30.0	28.0 27.2 29.1	28.1	93.7	3.39
Human serum	30.0	33.4 31.7 31.5	32.2	107.3	3.24



the free-label sensor possesses robust photostability, outstanding selectivity, satisfactory reproducibility, and remarkable applicability for  $\mu$ PAD analysis and water samples. It is expected that these SUCNPs may be applied in other analytical fields.

## Conflicts of interest

There are no conflicts to declare.

## Acknowledgements

We appreciate the support of the Natural Science Foundation of Jiangsu Province (BK20191041), the National Natural Science Foundation of China (21535003, 21575022), and funding for School-Level Research Projects of Yancheng Institute of Technology (xjr2019020, xjr2019021).

## Notes and references

- 1 X. Yue, J. Wang, J. Han, B. Wang and X. Song, *Chem. Commun.*, 2020, **56**, 2849–2852.
- 2 Q. Xu, C. H. Heo, J. A. Kim, H. S. Lee, Y. Hu, D. Kim, K. M. Swamy, G. Kim, S. J. Nam, H. M. Kim and J. Yoon, *Anal. Chem.*, 2016, **88**, 6615–6620.
- 3 P. Chen, Z. Zheng, Y. Zhu, Y. Dong, F. Wang and G. Liang, *Anal. Chem.*, 2017, **89**, 5693–5696.
- 4 X. Zhong, Q. Yang, Y. Chen, Y. Jiang, B. Wang and J. Shen, *J. Mater. Chem. B*, 2019, **7**, 7332–7337.
- 5 Y. Pang, Y.-K. Huang, F. Li, F.-Q. Yang and Z.-N. Xia, *Anal. Methods*, 2016, **8**, 6545–6553.
- 6 D. Han, M. Qian, H. Gao, B. Wang, H. Qi and C. Zhang, *Anal. Chim. Acta*, 2019, **1074**, 98–107.
- 7 B. Endrödi, A. Stojanovic, M. Cuartero, N. Simic, M. Wildlock, R. de Marco, G. A. Crespo and A. Cornell, *ACS Sustainable Chem. Eng.*, 2019, **7**, 12170–12178.
- 8 S. Apoorva, P. Behera, B. Sajjanar and M. Mahawar, *Mol. Biol. Rep.*, 2020, **47**, 2231–2242.
- 9 Y. Han, W. Lv, H. Chen, H. Li, J. Chen, Z. Li and H. Qiu, *Anal. Chem.*, 2020, **92**, 3949–3957.
- 10 Z. Wei, H. Li, S. Liu, W. Wang, H. Chen, L. Xiao, C. Ren and X. Chen, *Anal. Chem.*, 2019, **91**, 15477–15483.
- 11 Z. X. Wang, X. Jin, Y. F. Gao, F. Y. Kong, W. J. Wang and W. Wang, *Mikrochim. Acta*, 2019, **186**, 328.
- 12 H.-X. Yu, J. Zhi, T. Shen, W. Ding, X. Zhang and J.-L. Wang, *J. Mater. Chem. C*, 2019, **7**, 8888–8897.
- 13 J. Wu, L. Jiang, P. Verwilt, J. An, H. Zeng, L. Zeng, G. Niu and J. S. Kim, *Chem. Commun.*, 2019, **55**, 9947–9950.
- 14 Z. X. Wang and S. N. Ding, *Anal. Chem.*, 2014, **86**, 7436–7445.
- 15 Z.-X. Wang, Y.-F. Gao, X.-H. Yu, F.-Y. Kong, W.-X. Lv and W. Wang, *Microchim. Acta*, 2018, **185**, 422.
- 16 Z.-X. Wang, X.-H. Yu, F. Li, F.-Y. Kong, W.-X. Lv and W. Wang, *J. Mater. Chem. B*, 2018, **6**, 1771–1781.
- 17 Y. F. Gao, X. Jin, F. Y. Kong, Z. X. Wang and W. Wang, *Analyst*, 2019, **144**, 7283–7289.
- 18 O. Ola, Y. Chen, K. Thummavichai and Y. Zhu, *Sustainable Energy Fuels*, 2020, **4**, 5223–5228.
- 19 Z. X. Wang, Y. F. Gao, X. H. Yu, F. Y. Kong, W. J. Wang, W. X. Lv and W. Wang, *Analyst*, 2019, **144**, 550–558.
- 20 X. Zhang, Y. Chen and S.-N. Ding, *Sci. Bull.*, 2017, **62**, 1256–1266.
- 21 Y. Dong, Y. Chen, X. You, W. Lin, C. H. Lu, H. H. Yang and Y. Chi, *Nanoscale*, 2017, **9**, 1028–1032.
- 22 L. Li, D. Liu, H. Mao and T. You, *Biosens. Bioelectron.*, 2017, **89**, 489–495.
- 23 R. Hu, L. Li and W. J. Jin, *Carbon*, 2017, **111**, 133–141.
- 24 Z.-X. Wang, F.-Y. Kong and W. Wang, *Chem.-Eur. J.*, 2017, **23**, 665–675.
- 25 E. Eshelman, M. G. Daly, G. Slater, P. Dietrich and J. F. Gravel, *Planet. Space Sci.*, 2014, **93–94**, 65–70.
- 26 L. Zhao, T. Cai, M. Ye, D. Liu and S. Liu, *Carbon*, 2019, **150**, 319–333.
- 27 E. S. Seven, S. K. Sharma, D. Meziane, Y. Zhou, K. J. Mintz, R. R. Pandey, C. C. Chusuei and R. M. Leblanc, *Langmuir*, 2019, **35**, 6708–6718.
- 28 S. Sidhik, J. Velusamy, E. De la Rosa, S. A. Pérez-García, G. Ramos-Ortiz and T. López-Luke, *Carbon*, 2019, **146**, 388–398.
- 29 C. Lu, Q. Zhu, X. Zhang, H. Ji, Y. Zhou, H. Wang, Q. Liu, J. Nie, W. Han and X. Li, *ACS Sustainable Chem. Eng.*, 2019, **7**, 8542–8553.
- 30 T. Dey, S. Mukherjee, A. Ghorai, S. Das and S. K. Ray, *J. Phys. Chem. C*, 2020, **124**, 12161–12167.
- 31 Z. Xu, X. Sun, P. Ma, Y. Chen, W. Pan and J. Wang, *J. Mater. Chem. C*, 2020, **8**, 4557–4563.
- 32 X. Gao, C. Du, Z. Zhuang and W. Chen, *J. Mater. Chem. C*, 2016, **4**, 6927–6945.
- 33 Q. Wang, W. Wang, J. Lei, N. Xu, F. Gao and H. Ju, *Anal. Chem.*, 2013, **85**, 12182–12188.
- 34 J. Bartelmess, S. J. Quinn and S. Giordani, *Chem. Soc. Rev.*, 2015, **44**, 4672–4698.
- 35 S. Wang, S.-H. Wu, W.-L. Fang, X.-F. Guo and H. Wang, *Dyes Pigm.*, 2019, **164**, 7–13.
- 36 L.-S. Li, X.-Y. Jiao, Y. Zhang, C. Cheng, K. Huang and L. Xu, *Sens. Actuators, B*, 2018, **263**, 426–435.
- 37 K. Radhakrishnan and P. Panneerselvam, *RSC Adv.*, 2018, **8**, 30455–30467.
- 38 Y. Gong, B. Yu, W. Yang and X. Zhang, *Biosens. Bioelectron.*, 2016, **79**, 822–828.
- 39 E. F. C. Simões, J. M. M. Leitão and J. C. G. E. da Silva, *Microchim. Acta*, 2016, **183**, 1769–1777.
- 40 B. Yin, J. Deng, X. Peng, Q. Long, J. Zhao, Q. Lu, Q. Chen, H. Li, H. Tang, Y. Zhang and S. Yao, *Analyst*, 2013, **138**, 6551–6557.
- 41 Q. Wang, C. Tan and W. Cai, *Analyst*, 2012, **137**, 1872–1875.
- 42 Z. Ding, C. Wang, G. Feng and X. Zhang, *ACS Omega*, 2018, **3**, 9400–9406.
- 43 H. Liu, Y. Sun, Z. Li, J. Yang, A. A. Aryee, L. Qu, D. Du and Y. Lin, *Nanoscale*, 2019, **11**, 8458–8463.
- 44 B. Valeur and I. Leray, *Coord. Chem. Rev.*, 2000, **205**, 3–40.

